Applied Geochemistry
December 2019, Volume 111 Pages 104440 (11p.)
https://doi.org/10.1016/j.apgeochem.2019.104440
https://archimer.ifremer.fr/doc/00566/67784/

Copper, zinc and lead isotope signatures of sediments from a mediterranean coastal bay impacted by naval activities and urban sources

Ferreira Araujo Daniel [1, *] , Ponzevera Emmanuel [1], Briant Nicolas [1], Knoery Joel [1], Bruzac Sandrine [1], Sireau Teddy [1], Brach-Papa Christophe [2]

[1] Laboratoire de Biogéochimie des Contaminants Métalliques, Ifremer, Centre Atlantique, F44311, Nantes Cedex 3, France
[2] Laboratoire Environnement Ressources Provence-Azur-Corse, Ifremer, Centre Méditerranée, Zone Portuaire de Brégaillon, CS20 330, 83507, La Seyne-sur-Mer Cedex, France

* Corresponding author : Daniel Ferreira Araujo, email address : danielunb.ferreira@gmail.com

Abstract :

Toulon bay is severely impacted by metal contamination induced by past and recent naval activities. In this work, Cu, Zn and Pb isotope compositions and elemental concentrations of fifty-five surface sediments were determined in order to map the spatial distribution of anthropogenic and natural sources along this land-sea continuum. Two sub-systems of Toulon Bay, the Small and Large bays, showed well-marked patterns on metal contamination levels and isotope signatures for Cu and Pb. The Small bay had the highest metal concentrations, and displayed average Pb and Cu isotope compositions of 1.1664 ± 0.0043 (1s, expressed as 206Pb/207Pb ratios) and −0.17 ± 0.19‰ (1s, expressed as δ65CuNIST values), respectively. It contrasted with the Large bay, with moderate to pristine metal concentrations and average Pb and Cu isotope compositions of 1.1763 ± 0.0079 (1s) and +0.08 ± 0.23‰ (1s), respectively. Lead isotope systematics indicated a binary source mixing process involving industrial and natural sources, while Cu isotope systematics showed a ternary mixing process involving two distinct anthropogenic signatures, interpreted as associated to new diffuse anthropogenic sources and old warfare material. In contrast, Zn isotope compositions in the Small and Large bays were practically the same: +0.06 ± 0.05‰ and +0.06 ± 0.11‰ (1s, expressed δ66ZnJMC values), respectively, denoting an overlap between isotope signatures of natural and anthropogenic sources. This study presents the first detailed spatial distributions of Cu and Zn isotope compositions for an aquatic system, and demonstrates the feasibility to use Cu isotopes as tracers of anthropogenic sources in coastal environments.

Highlights

► Cu isotope systematic show a mixing process of natural and anthropogenic sources. ► Low Cu contaminated sediments display $\delta^{65}Cu_{NIST}$ values ranging from 0.0 to +0.2‰. ► Contaminated sediments by diffuse sources tend to negative $\delta^{65}Cu_{NIST}$ values. ► Pb isotopes reveal mixing process involving industrial and natural sources. ► Zn isotope system does not allow identifying mixing source processes.

Keywords : metal isotopes, isotope tracers, geochemical isotopes, environmental pollution, coastal pollution, Toulon Bay

1. Introduction

The trace metal contamination of coastal systems, notably by copper (Cu), zinc (Zn) and lead (Pb), is a global environmental problem that imposes major risks for human health and ecological damages (Barletta et al., 2019; de Souza Machado et al., 2016; Naser, 2013). Toulon bay (NW Mediterranean Sea) is an emblematic coastal environment severely impacted by a multi-metallic contamination for Cu, Zn, Pb, As, and Hg originating from legacy to present recent naval and seashore human activities (marinas, industry, ship-building and maintenance, Navy). While a large load of these contaminants was released into the bay during the Second World War (WWII) as result of the French Navy fleet bombardment and scuttling (Tessier et al., 2011; Grasset, 2011), it has been reported trends of increasing on metal releasing by diffuse sources, including urban effluents, industry and anti-fouling paints (Coclet et al., 2018; Cossa et al., 2014; Dang et al., 2015a,b; Jean et al., 2012; Pougnet et al., 2014; Tessier et al., 2011).

Metal inputs of Cu, Zn and Pb into the bay since-WWII period are estimated to be about 595, 1091 and 817 tons respectively (Tessier et al., 2011). Most part of this stock (about 80%) rests confined in sediments along the military and civils ports of the bay, favored by the long water residence time and low hydrodynamic energy (Tessier et al., 2011). However, the rest of this metal inventory (~ 20%) is accessible to resuspension and transport toward the open sea associated to sediment particles (Dang et al., 2015a). This availability imposes major ecological and health risks to marine trophic webs and to local aquaculture activities, like as fishing and aquaculture farming (Dang et al., 2015b; Rossi and Jamet, 2008). Thus, understanding the origin of metal sources, pathways and sinks in this ecosystem are of upmost priority to develop effective environmental management, policy strategies, and monitoring programs.

To get a better appreciation of spatial distribution of sources and dynamics of metal contaminants, we combined complementary information from the stable isotopes of copper (^{63}Cu, ^{65}Cu), zinc (^{64}Zn, ^{66}Zn, ^{67}Zn, ^{68}Zn) and radiogenic Pb isotopes (^{206}Pb, ^{207}Pb, ^{208}Pb) in conjunction with a high-resolution surface sediment sampling in Toulon bay. The variability of Pb isotope compositions in environmental samples is induced by the radioactive decay of uranium (U) and thorium (Th) radionuclides and depends on the initial proportion between the parental and radiogenic nuclides (Komárek et al., 2008). The magnitude of lead isotope fractionation due to natural and anthropic processes is negligible in comparison to variations induced by U and Th decay. Thus, Pb isotope ratios (eg., ^{206}Pb/^{207}Pb) are conservative through biogeochemical processes (Komárek et al., 2008). Therefore, their ratios are convenient environmental tracers in the diverse or multiple pollution contexts like the urban atmosphere (Souto-Oliveira et al., 2019, 2018), mining operations and metallurgy (Dolgopolova et al.,

2006), urban sewage, and agricultural practices (Charalampides and Manoliadis, 2002). Zinc isotopes fractionate significantly during redox and evaporation processes during ore refining (smelting and electroplating industry), and coal combustion (Gonzalez and Weiss, 2015; Kavner et al., 2008; Yin et al., 2015). This results in zinc manufactured products and byproducts being isotopically distinct from their natural compartments (Gonzalez and Weiss, 2015; Shiel et al., 2010; Sivry et al., 2008), allowing to trace Zn anthropogenic inputs and their transfers in the sediment-water-biota interfaces (Araújo et al., 2016; 2017a,b; 2018, 2019). Unlike Zn, Cu does not fractionate during smelting ore refining due its high boiling point (2562 °C). Manufactured, slag and other metallurgical by-products inherit the isotope signature of Cu ore concentrates (Šillerová et al., 2017). As Cu isotope compositions of minerals formed in high temperature (>250 °C) - such as chalcopyrite, $CuFeS_2$ - are different from low temperature (<100°C) minerals - such as chalcocite, Cu_2S- , Cu has become a promising tool to trace origins of archeological materials and archeometallurgical processes (Jansen et al., 2018; Klein et al., 2009). Since anthropogenic Cu may derive either from sulfides or oxide ore deposits, Cu isotope systematics can help discriminate the different anthropogenic and natural sources. In environmental studies, Cu isotopes have been a useful tracer in urban aerosol samples (Souto-Oliveira et al., 2019, 2018) and in surrounding soils impacted by metallurgical (Mihaljevič et al., 2019; Šillerová et al., 2017) and vineyard activities (Babcsányi et al., 2016; El Azzi et al., 2013), however their applicability in complex and reactive aquatic systems has been more challenging (Araújo et al., 2019; Petit et al., 2013; Viers et al., 2018).

The particular feature of Toulon bay with anomalous metal enrichment in nearshore sediments contrasting against more pristine offshore sediments, provides a unique opportunity to test a multi-isotope approach (Cu-Zn-Pb) as an environmental forensic tool able to deconvolute spatial source distribution of metal and inferring dispersion mechanisms for these contaminants along the land-sea continuum.

2. Materials and methods

2.1 Study area and sampling

Toulon Bay is an urbanized French coastal ecosystem of approximately 600,000 inhabitants separated from the open sea to the East and South by the peninsula of Giens, and St.Mandrier, respectively (Tessier et al., 2011, Fig. 1). Two main urban rivers bring freshwater into this bay: the Las and Eygoutier rivers (Misson et al., 2016, Fig.1). A seawall built in the 19th century nearly isolates two sub-basins labelled the “Small bay” (9.8 km^2, semi-enclosed),

on the northwestern side, and "Large bay" (42.2 km^2), on the southeastern part (Fig. 1). On the Small bay shore are located urbanized areas, an arsenal and military port, industrial, recreational and commercial ports and former shipyards (closed in 1989). The Large bay is open to Mediterranean Sea to its east, and hosts a single military zone and several small beaches and tourist ports. A wastewater treatment plant releases treated effluent to the open sea close to sampling point 34 (Fig.1), and a second in the western, outer part of the Bay (Cap Sicié, not visible in Fig. 1).

Fifty-five sampling sites of surface sediment (0-5 cm) were considered to this study (Fig.1), accounting for twenty-four sites in the Small bay (Cs, Mis, Petite Mer, SMS and Stations 1-19) and twenty-eight in the Large bay (Stations 21-52). The samples were collected between November 2008 and June 2009 in the frame of the CARTOCHIM project driven by the PROTEE laboratory at the University of Toulon. They were characterized for their trace metal concentrations and Pb isotopes (Dang et al., 2015b; Tessier et al., 2011), Sn and butyl-Sn species in previous studies (Pougnet et al., 2014). Here, new aliquots from the same sediment samples were dissolved for trace elements and Cu, Zn and Pb isotope analyses.

2.2 Sample preparation and instrumental analysis

All reagents, labware acid cleaning and solution dilutions for elemental and isotope analyses were performed using 18.2 $M\Omega.cm^{-1}$ H_2O (Nanop System®) and ultra-pure acids (PlasmaPure *Plus* grade, SCP science®). Unsieved dry aliquots of sediments were digested in Teflon® bombs on a coated graphite block using multiple-step acid procedure with HF, HCl and HNO_3. The final extract solution was split for subsequent elemental and isotope analyses. Procedural blanks and international certified reference materials (MESS-3 and PACS-2 from NRC – CNR®) were processed in each batch of sediment samples and followed the complete procedure (digestion, elemental analysis, ion chromatography and isotope measurements). Elemental concentrations of Cu, Zn, Pb, Cd, Ag, Ni, Co, Cr, V, Li, Mn, Al and Fe were determined by inductively coupled plasma mass spectrometry (Q-ICP-MS, iCAP Qc, Thermo Fisher Scientific) at the Laboratoire de Biogéochimie des Contaminants Métalliques (LBCM, Ifremer, Nantes). The accuracy, as average bias, was always within 10% of the certified values of both reference materials for considered elements. Lead isotope ratio ($^{206}Pb/^{207}Pb$ and $^{208}Pb/^{206}Pb$) measurements were performed with the same instrument. Mass bias and instrumental drift were corrected with a standard bracketing method using the NIST SRM-981 standard reference material. The $^{206}Pb/^{207}Pb$ and $^{208}Pb/^{206}Pb$ internal relative standard deviations average were of 0.20 ±0.07% and 0.47±0.17% (1s, n = 60), respectively, for

unknown samples and sediment reference materials (MESS-3 and PACS-2). Lead isotope ratios obtained for the reference materials are included in the Table 1S (Supplementary Material).

For isotope analysis, Zn and Cu were isolated from matrix elements by ion-exchange chromatography technique adapted from protocol of Maréchal *et al*. (1999). The whole chromatography procedure was performed in an overpressured air-filtered cleanroom (Class 1000) at the *Laboratoire de Biogéochimie des Contaminants Métalliques* (LBCM, Ifremer, Nantes).The recovery yields (around 100 ±10%) were systematically checked by ICP-MS at the same laboratory. The total procedural blanks were below 1% of Zn and Cu mass content of the samples. Copper and Zinc isotopes were measured at the Pôle Spectrométrie Océan (Ifremer, Brest, France) using MC-ICP-MS (Neptune, Thermo Scientific). Samples were dissolved in 2% (v/v) HNO_3 and introduced at concentrations between 100 and 300 $ng.g^{-1}$ with a stable introduction system (SIS: cyclonic spray chamber) and a low flow PFA nebulizer (50 $\mu L.min^{-1}$). The final isotope compositions are expressed as $\delta^{65}Cu$ and $\delta^{66}Zn$ values in relation to NIST SRM 976 and to the "JMC-Lyon" (Johnson Matthey Company 3-0749-L), respectively, as follow:

$$\delta^{66/64}Zn_{JMC}\ (‰) = \left(\frac{R\left(\frac{^{66}Zn}{^{64}Zn}\right)_{sample}}{R\left(\frac{^{66}Zn}{^{64}Zn}\right)_{JMC}} - 1 \right) x\ 1000 \quad \text{(Eq.1)}$$

$$\delta^{65/63}Cu_{NIST\ 976}\ (‰) = \left(\frac{R\left(\frac{^{65}Cu}{^{63}Cu}\right)_{sample}}{R\left(\frac{^{65}Cu}{^{63}Cu}\right)_{NIST\ 976}} - 1 \right) x\ 1000 \quad \text{(Eq.2)}$$

Sediment reference materials measured three times along each analytical session were used for analytical quality control. The $\delta^{65}Cu_{NIST}$ and $\delta^{66}Zn_{JMC}$ average values obtained for marine sediments (MESS-3 and PACS-2) are reported in the Table 1S. External precision (2s) average obtained from two to three measurements of unknown samples and sediment certified materials was ±0.05‰ and ±0.06‰ for $\delta^{65}Cu_{NIST}$ and $\delta^{66}Zn_{JMC,}$ respectively. This corresponds to the uncertainty bars presented in the data plots (Fig. 5 and 6).

2.3 Enrichment Factor

The Enrichment Factor (EF) of trace metals is an index used to estimate the degree of anthropogenic contamination. Dilution effects related to grain size and mineralogical heterogeneities are decreased by the normalization of a metal concentration in the sample to the concentration of a reference element (Chen et al., 2009). In this work, aluminum (Al) was used as reference element and EF values were calculated as follows:

$$EF = \left(\frac{(\mathrm{M/Al})_{\mathrm{Sample}}}{(\mathrm{M/Al})_{\mathrm{background}}}\right) \text{(Eq.3)}$$

where "M" is the concentration of the metal of interest and "Al" is the reference element concentration, whereas "$(M/Al)_{sample}$" represents the concentration ratio in the sample and "$(M/Al)_{background}$" refers to the concentration ratio considered as free of anthropogenic influence, i.e., the representative of natural background. In this work, the sample station 31 was chosen as a representative natural sample based on its Pb isotope compositions ($^{206}Pb/^{207}Pb$ = 1.1998, Table 1S), which is consistent with natural Pb isotope signatures referred in previous studies performed in Toulon bay ($^{206}Pb/^{207}Pb_{natural}$ = 1.195; Dang et al., 2015b). EF values were classed as suggested in other studies (Chen *et al.,* 2007): EF < 1 indicates no enrichment; EF < 3 is minor enrichment; EF = 3–5 is moderate enrichment; EF = 5–10 is moderately severe enrichment; EF = 10–25 is severe enrichment; EF = 25–50 is very severe enrichment; and EF > 50 is extremely severe enrichment.

2.4 Statistics and geostatistical methods

All descriptive and multivariate statistics were performed using the SPSS® software v.18.0 (IBM®). Principal Component Analysis (PCA) was applied as exploratory tool to examine and identify the main interrelations among the isotope and elemental variables. PCA is useful for simplifying or extracting main dataset information by grouping inter-correlated variables in a smaller number of underlying factors, also known as principal components (Meglen, 1992). Before run PCA, linearity of variables was checked by scatter plots, while sampling adequacy of the dataset and its suitableness for data reduction was validated with the Kaiser-Meyer-Olkin (KMO) index and Bartlett's test, respectively. PCA factor loads were calculated using the correlation matrix with varimax rotation. Factor loads express the influence of each variable in the principal components (Field, 2017). The sample factor scores were calculated using the regression method to assess the influence of each component in individual samples (Field, 2017; Araújo et al., 2017c;). The principal components (PCs) that had

eigenvalues higher than 1 were selected for discussion (Mar da Costa et al., 2016; Mulholland et al., 2012). The communalities values of all variables equal or higher than 0.5 were used as thresholds for PCA results acceptance (Araújo et al., 2017c).

Interpolation maps were used for a better spatial visualization of elemental and isotope data and were performed using the Inverse Distance Weighting (IDW) method with ArcGIS® software v. 10.5(ESRI®). The IDW is the simplest interpolation method that uses the surrounding measured values to derive a prediction for an unmeasured location (Tessier et al., 2011).

3. Results and discussions

3.1 Enrichment factor values and spatial distribution of trace metals

All elemental isotope data for trace metals are presented in Table 1S (Supplementary Material). The calculated enrichment factors are shown in Table 2S (Supplementary Material). Copper, Zn, Pb, Ag and Cd present the highest enrichment factor values in sediments of Toulon bay (Fig. 2). In the Small bay, Zn, Ag, Pb reached severe enrichment levels ($10 < EF < 25$), while Cu and Cd presented a very severe enrichment ($25 < EF < 50$). EF decrease significantly for these elements in the Large bay (Fig.2), reaching levels of minor enrichment ($EF < 3$, for Zn, Ag, Pb, Cd) and moderate enrichment ($3 < EF < 5$, for Cu). It is noted in the Large bay two anomalous EF Cu values for the sampling stations 37 and 42 (Fig. 2).

The elements Li, V, Cr, Co and Ni display a homogenous distribution between the Small and Large bays, with low EF values (< 3). These low values indicate no enrichment or a minor enrichment, suggesting few or practically no anthropogenic influence (Fig. 2). Overall, Mn also displayed low EF values (< 3) through the bay, but with a noticeable enrichment in the Large bay (average EF of 1.70) in relation to Small bay (average EF of 0.9). This increase in Mn contents in surface sediments is apparent in the Fig.2. The most exceptional sampling stations are 37, 47, 50, reaching the highest Mn EF values ($3 < EF < 5$, Fig. 2).

PCA analysis identified two main components, together explaining 82% of total variance of all dataset. The PCA component plots (Fig.3a) provides a general pattern of metal associations in the Small and Large bays. Supported by EF values, these associations show that: (i) Cu, Zn, Pb, Ag and Cd represent elements of dominant anthropogenic origin and are grouped along the first component (x-axis); (ii) Li, Co, V, Cr and Ni represent elements predominantly issued from natural sources and are grouped along the second component (y-axis); and (iii) that Mn stands apart in relation to the other elemental groups representing an element of dominant

natural origin influenced by diagenetic processes. The diagenesis occurring in sediments under anoxic conditions in the Small bay reduces Mn oxyhydroxides to Mn(II), which is mobilized into the pore waters, and subsequently precipitating as Mn-oxides or carbonates in the dominant oxic conditions of the Large bay (Araújo et al., 2017c; Dang et al., 2015a). This diagenetic Mn remobilization from the Small bay toward the Large bay explains the well-marked Mn enrichment zones between these systems (Fig. 2).

The plot of sample factor scores (Fig.3b) allow verify the weight of each component obtained in the PCA analysis for individual sediment samples. For the surface sediments located in the Small bay, it is observed an association with elements of anthropogenic origin identified in the first component (Cu, Zn, Pb, Ag, Cd). On the other hand, both Small and Large bays present similar factor scores for the second component associated to natural elements (Li, Co, V, Cr and Ni). This reflects a homogenous natural metal baseline within the entire bay. Also, the associations and spatial distribution of trace metals match well with the spatial patterns of EF values observed in the maps of interpolation (Fig. 2). In summary, multivariate statistics and geostatistical approach shows a clear inter-bay contrast, highlighting the highest concentrations for Cu, Zn, Pb and Ag in the vicinity of civil and military ports with a strong punctual anomaly at the MIS station (collected inside the military zone). Moreover, an additional anthropogenic metal input coming from the basin drainage and delivered by the Las river water outlet is plausible.

In the following sections, Pb, Cu and Zn isotope systematics are discussed in order to characterize the natural and anthropogenic signatures and possibly to deconvolute potential multiple anthropogenic sources. Use of Cu and Zn stable isotopes as environmental tracers of surficial sediments requires that early diagenetic processes do not alter significantly source isotope records and that the sediment column remains undisturbed. Diagenetic reactions induced by microbial degradation of organic matter change redox conditions in sedimentary strata in the surrounding water, which in turn, promotes mineral dissolution or the formation of new mineral phases, including sulfides, carbonates and oxides (Machado et al., 2008; Mason, 2013). These mechanisms of adsorption of metals onto mineral surfaces, or in their inclusion in crystal lattices control their mobility and speciation and affect their isotope fractionation (Dekov et al., 2014; Ducher et al., 2016; Jamieson-Hanes et al., 2017; Ratié et al., 2015; Veeramani et al., 2015). In Toulon bay, earlier examination of sediments and porewaters demonstrated increases of trace metals concentrations (Co, Cu, Pb) due to such processes mediated by Mn and Fe oxyhydroxides reduction under anoxic conditions (Dang et al., 2015a). However, the metal loads delivered from sediments to the overlying water column account for

less than 1% of sediment pool, suggesting that changes of the Cu and Zn isotope compositions due to such biogeochemical processes are negligible. This is coherent with other studies that have also pointed out that Cu and Zn isotope compositions in bottom or particulate sediments are essentially controlled by source mixing processes (Araújo et al., 2017a; Babcsányi et al., 2014; Chen et al., 2009; Guinoiseau et al., 2018; Thapalia et al., 2015; Zhang et al., 2018). The second criterion based on integrity of the stratigraphy is met since geochemical profiles of these trace metals in dated cores of Toulon bay were consistent with historical events of metal contamination indicating a good preservation of geochemical records (Tessier et al., 2011).

From an ecological perspective, understanding the diagenesis effects on elemental speciation and bioavailability at sediment-water interface are of prime importance to determine the bioaccumulation routes of metals in the trophic chain. This can occur directly from the sediment, as in the case of benthic organisms living in the sediments, or by the dissolved fraction of interstitial surface waters, in the case of primary producers (phytoplankton, macrophytes and bacteria) (Ahlf et al., 2009; Briant et al., 2017; Chouvelon et al., 2018; Zhou et al., 2008; Zuykov et al., 2013). Then, a better understanding of the diagenesis influence on Cu and Zn isotope fractionation at sediment-water interface will be helpful to exploit the isotope records in biological tissues.

3.2 Pb isotope systematics

Bulk lead concentrations variated from 13 to 470 $\mu g.g^{-1}$, matching well with the previous concentration range reported by Tessier et al. (2011). The Small bay has an average Pb concentration of 144 $\mu g.g^{-1}$, while the Large bay has an almost threefold lower Pb concentration at around 49 $\mu g.g^{-1}$ (Table 1).

Lead isotope ratios ($^{206}Pb/^{207}Pb$) are ranging from 1.1591 to 1.1998 in the entire sediment dataset. Averages ratios of 1.1664 ±0.0043 and 1.1763 ±0.0079 are observed in the Small and Large bays, respectively (Table 1). The lowest $^{206}Pb/^{207}Pb$ ratio values found in sediments from the Small bay are close to the anthropogenic signature value proposed by Dang et al., 2015 ($^{206}Pb/^{207}Pb_{anthrop.}$ ~ 1.166 ±0.003, Fig. 4), while sediments from the Large bay tend to approximate a more natural baseline ($^{206}Pb/^{207}Pb_{natural}$ ~ 1.18 -1.20, Fig. 4). Plotting $^{206}Pb/^{207}Pb$ ratios *vs.* EF Pb values denotes a binary source mixing processes between natural and anthropogenic end members (Fig. 5a). The latter dominates in the Small bay and is attributed to multi-uses of Pb in the Navy and industrial activities (Dang et al., 2015b). The spatial interpolation map of $^{206}Pb/^{207}Pb$ ratios indicates a gradual attenuation of Pb contamination from

the Small bay toward the open sea, as a result of transport and dilution by natural particles (Fig. 4).

3.3 Cu isotope systematics

Copper concentrations range from 4.4 to 666 µg. g^{-1}, while $\delta^{65}Cu_{NIST}$ ranged between -0.79 and +0.34‰ (Table 1). In the Small bay, the average Cu concentration reach 147 µg. g^{-1} and an average $\delta^{65}Cu_{NIST}$ of -0.17 ±0.19‰ (1s), while in the Large bay, Cu concentration average is lower (ca. 32 µg. g^{-1}), and $\delta^{65}Cu_{NIST}$ tends to more positive and heavier values (+0.08 ±0.23‰, 1s).

The contrast between Cu isotopes fingerprints in sediments of Small and Large bays is noticeable in the Fig. 4. In the plot of $\delta^{65}Cu_{NIST}$ *vs.* 1/[Cu] (Fig. 5b) well-defined data clusters are identified for each bay. However, in both sub-bays isotopic outliers are observed: the Small bay clusters overall light Cu isotope compositions, but the sampling stations MIS ($\delta^{65}Cu_{NIST}$ = +019), Petit Mer ($\delta^{65}Cu_{NIST}$ = +0.01) and St.16 ($\delta^{65}Cu_{NIST}$ = +0.34) stand out with positive δ-values (Fig. 5b). In turn, the Large bay is most dominated by positive and narrow range of $\delta^{65}Cu_{NIST}$ values, from -0.04 to +0.24‰, but the negative δ-values of sampling St.25 ($\delta^{65}Cu_{NIST}$ = -0.22) and 26 ($\delta^{65}Cu_{NIST}$ = -0.79) diverge from the Large bay clustering data (Fig. 5b). In terms of EF Cu values, the St.37 and 42 differ from the rest of sediments of the Large bay. Unfortunately, we do not dispose of their Cu isotope compositions. Disregarding these outlier data, a general trend toward lighter $\delta^{65}Cu_{NIST}$ associated with an increase of Cu concentrations or EF Cu (Fig. 5c) is noticeable, which suggests a source mixing process involving anthropogenic and natural sources.

The overall positive and heavier $\delta^{65}Cu_{NIST}$ values and associated low Cu EF values in the Large bay reflect a dominant signature of natural Cu. As coastal sediments integrate inorganic and organic compounds derived from detrital and autochthonous materials – such as, clay minerals, amorphous solids, biogenic carbonates, organic debris- (Bianchi, 2007; de Souza Machado et al., 2016; Turner and Millward, 2002), a finer description of Cu speciation/partition and isotope compositions would require additional data characterization of samples (e.g. with synchrotron-based X-ray absorption). Fortunately, previous application of selective chemical leaching (ascorbate, acid dilute and alkaline solution) have already indicated that Fe/Mn oxy-hydroxides and sulphides are the main carrier phases controlling Cu mobility in Toulon bay (Dang et al., 2015). Clay minerals play this important role on Cu dynamics due to their abundance and high charge surface. In these solid phases, Cu may occur within the lattice of aluminosilicates, adsorbed on the surface of clays and amorphous solids or complexed by

organic matter (Sparks, 2005). As a trace component of silicates, Cu probably inherits the lithogenic Cu isotope composition close to the average of the Upper Continental Crust (UCC, +0.07± 0.10‰, Liu et al., 2015; Savage et al., 2015). For other carrier phases, laboratory experiments under controlled conditions show a preferential association of the heavy isotope into solid surfaces, such as oxy-hydroxides (Balistrieri et al., 2008; Pokrovsky et al., 2008) and organic complexes (Bigalke et al., 2010). Therefore, the natural Cu partition in sediments and associated isotope signatures of the Large bay seems consistent with previous field and laboratory findings reported in the literature.

On the other hand, the outlier $\delta^{65}Cu_{NIST}$ values corresponding to the sampling stations 25 and 26 are similar to the light isotope signatures found in the Small bay. This can be related to a zone of dredge spoils near St. Mandrier (Fig.1) or a preferential hydrodynamic deposition of fine particles enriched in contaminants in this area (Tessier et al. 2011). This area was used in the 1980's for contaminated spoils from the north of the Small bay. Subsequent transport and dispersion promoted by reworking and resuspension (large boat traffic, storm events) of the Cu-enriched dredged sediments could explain the anomalous value of -0.79 at St.26.

The dominant anthropogenic Cu signature in the Small bay (Fig. 4) tending to negative $\delta^{65}Cu_{NIST}$ values can result from the mixing of ancient and modern Cu anthropogenic sources by reworking of sediments. It potentially includes a broad spectrum of Cu materials employed in harbor and Navy activities, including alloys, plumbing, antifouling paints, warfare, etc.

In turn, the sample at MIS station, collected in the military harbor, and that presents the highest Cu concentration in the sampling grid, constitutes a remarkably punctual anthropogenic source with a positive $\delta^{65}Cu_{NIST} = +0.19 \pm 0.05$‰ (2s). The isotope signature could be attributed to the burning of warfare material enriched in Cu (explosives, driving bands, fuses and shell casings) during WWII. In 1942, The French Navy scuttled more than 70 ships including battleships, cruises, destroyers and submarines (Grasset, 2011) of its own navy fleet to avoid its capture by the Nazi forces (Grasset, 2011). It is evident that such source attribution requires additional Cu isotope characterization of ancient and modern industrialized materials as well historical information of manufacturing processes and ore purchasing. High contamination of Cu and other metals induced by bullet shells have been reported for battlefields of the Great War: in Verdun (France), burning of arsenic-containing shells resulted in anomalous concentrations in soils for Cu (9113 $\mu g.g^{-1}$), Pb (5777 $\mu g.g^{-1}$) and Zn (90190 $\mu g.g^{-1}$, Bausinger et al., 2007), while in the region around Ypres (Belgium) was estimated an input of 2800 t of Cu in the upper 0.5 m of soil due to shelling accumulation (Meirvernne et al., 2008). These

findings support our preliminary interpretation of Cu isotope signatures in the military zone of Toulon bay.

Similarly to "MIS" sample, the "Petite Mer" and "St.16" samples present also relatively heavy $\delta^{65}Cu_{NIST}$ values. However, Petite Mer sample has a very low Cu content (ca. 15 $\mu g.g^{-1}$, EF Cu = 1.9) and a typical radiogenic $^{206}Pb/^{207}Pb$ ratio (1.1801), which supports a natural Cu origin, as lattice component of minerals. A possible explanation for its heavy $\delta^{65}Cu_{NIST}$ and low Cu concentration value would be a granulometry effect associated to coarser mineral grains (e.g, quartz) with low mineral surface charge that sorbs anthropogenic Cu (Sparks, 2005). Instead, the sampling St.16 (c.a, 44, $\mu g.g^{-1}$, EF Cu = 5.0) is moderately enriched, suggesting that its heavy $\delta^{65}Cu_{NIST}$ value (+0.34‰) reflects an anthropogenic origin. Several sedimentary archives studied previously by Dang *et al.* 2015a have showed a remarkable peak of Cu concentration corresponding to WWII events followed by a continuous decreasing of Cu inputs in the period post-WWII. However, the sediment core collected near this zone presented no attenuation of Cu concentrations in the profile. This could be explained by sediment reworking of Cu-enriched layers and mixing of Cu isotope compositions related to past events of WWII impacts. Alternatively, a punctual unknown anthropogenic source cannot be discarded. A temporal analysis of Cu isotopes will be useful to discriminate past and present anthropogenic inputs, and hence, elucidating this question.

3.4 Zn isotope systematic

Zinc concentrations varied from 19 to 1471 µg. g^{-1}, while $\delta^{66}Zn_{JMC}$ ranged from -0.27 to +0.28‰ (Table 1, Fig. 4). Unlike Cu and Pb isotope systems, Zn isotope compositions in the Small and Large bays greatly overlap: +0.06 ±0.05 (1s) and +0.06 ±0.11(1s), respectively. Indeed, $\delta^{66}Zn_{JMC}$ and Zn concentrations do not correlate (Fig. 6a) neither in the Small or Large bay, limiting interpretations in terms of source mixing processes. Interestingly, Zn concentrations correlate very well with Pb concentrations and $^{206}Pb/^{207}Pb$ ratios (Fig. 6b,c). This allows using Pb isotopes to identify the best representative Zn anthropogenic and Zn natural samples. Using the Pb isotope ratios associated to natural ($^{206}Pb/^{207}Pb$ ~ 1.180) and anthropogenic ($^{206}Pb/^{207}Pb$ ~ 1.165) sources as cut-off lines (Fig. 6d), we sort them in two groups. The natural Zn samples with Zn concentrations lower than 60 $\mu g.g^{-1}$ and a $\delta^{66}Zn_{JMC}$ average of +0.14 ±012 ‰ (2s, n= 9), and anthropogenic Zn samples with average concentrations of 383 $\mu g.g^{-1}$ and $\delta^{66}Zn_{JMC}$ values of +0.04±0.08 ‰ (2s, n= 12). These $\delta^{66}Zn_{JMC}$ values estimated as the best representative of natural and anthropogenic Zn sources are statically equal (test *t*, p

>0.5) and show an overlap between isotope signatures of natural and anthropogenic sources in Toulon bay.

It is noted that the estimated anthropogenic $\delta^{66}Zn_{JMC}$ values of +0.04 ±0.08 (2s, n= 12) are close to the isotope range reported for Zn sulfide (from +0.13 to +0.15‰) and silicates ores (−0.06 to +0.41‰, (Mondillo et al., 2018), and are clearly distinguished from those attributed to industrial atmospheric emissions (< -0.6‰, Souto-Oliveira *et al.*, 2018; from –0.52 to +0.02‰, Mattielli *et al.*, 2009; from -0.27 to +0.15‰, Ochoa *et al.*, 2016; from +0.16 to +0.63‰, Cloquet *et al.*, 2006), or slags ($\delta^{66}Zn$ > 0.5‰, Yin *et al.*, 2005; Araújo et al., 2017a,b). The final refined Zn metal (Zn^0) approximates the average Zn isotope composition of ores (John et al., 2007), when Zn processing yields in metallurgical plants are higher than 95% (Sivry et al., 2008; Yin et al., 2015). This implies that Zn anthropogenic signatures of alloys used in shipyard or in shells are similar and thus, not discriminable by Zn isotopes (John et al., 2007; Yin et al., 2015).

Natural Zn inputs in coastal systems are associated to inorganic particles issued from weathered soils and lithogenic materials, detrital and authigenic organic matter and in-situ formed minerals, as carbonates and solid sulfide minerals (Araújo et al., 2017a; Mortimer and Rae, 2000; Zhang et al., 2018). The detrital-inorganic materials dominate sediment compositions of Toulon bay. However, the estimated natural $\delta^{66}Zn_{JMC}$ values of +0.14 ±0.12‰ are slightly lighter than the Zn isotopes values reported to the Upper Earth Crust, estimated as +0.28 ±0.05‰ (Chen et al., 2013) and other unpolluted sediments from estuaries worldwide: (+0.28‰, Sepetiba bay, Araújo et al., 2017a; +0.3‰, Gironde estuary, Petit et al., 2015 ; +0.3‰, the Loire estuary, Araújo et al., 2019). This slight enrichment in light isotopes could be attributed to the regional geology.

Overall, igneous, sedimentary and metamorphic rocks worldwide present homogenous isotope compositions clustering around +0.2 to +0.3‰ (Moynier et al., 2017), but discrete and detectable Zn isotope heterogeneities on geological settings may occur as result of magmatic differentiation, weathering, crustal subduction processes, mantle melting and volcanisms, and past biological activity (Chen et al., 2013; Doucet et al., 2018; Inglis et al., 2017; John et al., 2017; Kunzmann et al., 2013; Lv et al., 2016; Wang et al., 2017). Recent studies have demonstrated how Zn isotope heterogeneity in the continental lithosphere is useful to elucidate petrogenesis evolution, e.g, for discriminating the influence of differentiation processes from melting products in felsic rocks (Doucet et al., 2018). The local geology of Toulon bay basin encompasses mainly Permian and Triassic sediments, Paleozoic metamorphic rocks (www.geoportail.gouv.fr). Evoking possible mechanism of Zn isotope fractionation during

high-temperature such as magmatic differentiation could explain this slight tendency to lighter isotope values in the local geology of Toulon bay. Alternatively, this light Zn isotope geochemical baseline of sediments of Toulon bay could be associated to the contribution of sedimentary rocks sources. Weathering processes occurring in the formation of these rocks lead to the progressive breakdown of primary minerals and the associated formation of phyllosilicates and iron oxides depleted in Zn content (Suhr et al., 2018). Changes on Zn-mineral bearing phases combined with biotically- and kinetically-controlled sorption reactions in Fe-oxyhydroxides and clay minerals surfaces could explain the enrichment of light Zn isotopes present in the weathered residual material (Guinoiseau et al., 2017, 2016; Little et al., 2014; Suhr et al., 2018). In turn, the heavy Zn isotope would be leached and enriched in the dissolved phase (Little et al., 2016). Further studies focused in the Mediterranean French geology will be helpful to establish the baseline of Zn isotopes in the region.

4. Conclusions

Toulon bay surface sediments present a remarkably anthropogenic contamination for Cu, Zn, Pb, Ag and Cd elements. Overall, these anthropogenic elements display a similar spatial distribution in the Toulon sub-bays, with the highest levels of contamination occurring in the Small bay and the lowest in the Large bay. Multivariate and geostatistics approaches show a clear inter-bay differences, highlighting the highest concentrations for Cu, Zn, Pb and Ag in proximity to civil and military ports and the Las river outlet. However, these methods cannot deconvolute the multiple origins of Pb, Zn, and Cu.

The Pb isotope systematics indicate a binary source mixing process involving industrial and natural sources, while Cu isotope records discriminated, at least two distinct anthropogenic signatures, preliminarily interpreted as associated to shipyard alloys and warfare materials. In turn, Zn isotope composition of natural and anthropogenic sources overlap. For Zn, analysis of specifics mineral phases of sediments rather than bulk could be more effective to decipher its natural and anthropogenic origins.

This study presents the first detailed spatial distribution of Pb, Cu and Zn isotope compositions for an aquatic system and demonstrates the use of Cu isotopes as tracers of anthropogenic sources in coastal environments. Considering the crucial role of surface sediments in the transfer of metal contaminants to water column and biota, this first isotope characterization will be useful to track the metal contaminant pathways from abiotic compartments to marine food webs in future studies. Further investigations on Cu, Zn and Pb isotope compositions of surface sediments will be useful to identify potential new

anthropogenic inputs, and thus, to better assess the change of source apportionment since WWII.

Acknowledgements

This work was conducted within the framework of the POLLUSOLS and SCOTTTI projects. They were funded by the regional government of the Pays de la Loire (France) and AERMC (*Agence de l'Eau Rhône Méditerranée Corse*), respectively. A part of this research is also a contribution to the MERMEX-Merite research program. This study benefits from sediment sample collection occurring from the CARTOCHIM project funded by "Toulon-Provence-Méditerranée (TPM)", and Agence de L'Eau Rhône Méditerranée Corse. The authors thank the anonymous reviewers for their helpful suggestions and comments on earlier drafts of the manuscript.

references

Ahlf, W., Drost, W., Heise, S., 2009. Incorporation of metal bioavailability into regulatory frameworks—metal exposure in water and sediment. *J Soils Sediments* 9, 411–419. https://doi.org/10.1007/s11368-009-0109-6

Araújo, D., Machado, W., Weiss, D., Mulholland, D.S., Boaventura, G.R., Viers, J., Garnier, J., Dantas, E.L., Babinski, M., 2017b. A critical examination of the possible application of zinc stable isotope ratios in bivalve mollusks and suspended particulate matter to trace zinc pollution in a tropical estuary. *Environmental Pollution* 226, 41–47. https://doi.org/10.1016/j.envpol.2017.04.011

Araújo, Daniel F., Boaventura, G.R., Machado, W., Viers, J., Weiss, D., Patchineelam, S.R., Ruiz, I., Rodrigues, A.P.C., Babinski, M., Dantas, E., 2017a. Tracing of anthropogenic zinc sources in coastal environments using stable isotope composition. *Chemical Geology* 449, 226–235. https://doi.org/10.1016/j.chemgeo.2016.12.004

Araújo, D.F., Boaventura, G.R., Viers, J., Mulholland, D.S., Weiss, D., Araújo, D., Lima, B., Ruiz, I., Machado, W., Babinski, M., Dantas, E., 2016. Ion Exchange Chromatography and Mass Bias Correction for Accurate and Precise Zn Isotope Ratio Measurements in Environmental Reference Materials by MC-ICP-MS. *Journal of the Brazilian Chemical Society*. https://doi.org/10.5935/0103-5053.20160167

Araújo, D.F., Machado, W., Weiss, D., Mulholland, D.S., Garnier, J., Souto-Oliveira, C.E., Babinski, M., 2018. Zinc isotopes as tracers of anthropogenic sources and biogeochemical processes in contaminated mangroves. *Applied Geochemistry* 95, 25–32. https://doi.org/10.1016/j.apgeochem.2018.05.008

Araújo, Daniel Ferreira, Peres, L.G.M., Yepez, S., Mulholland, D.S., Machado, W., Tonhá, M., Garnier, J., 2017c. Assessing man-induced environmental changes in the Sepetiba Bay (Southeastern Brazil) with geochemical and satellite data. *Comptes Rendus Geoscience* 349, 290–298. https://doi.org/10.1016/j.crte.2017.09.007

Araújo, D.F., Ponzevera, E., Briant, N., Knoery, J., Sireau, T., Mojtahid, M., Metzger, E., Brach-Papa, C., 2019. Assessment of the metal contamination evolution in the Loire estuary using Cu and Zn stable isotopes and geochemical data in sediments. *Marine Pollution Bulletin* 143, 12–23. https://doi.org/10.1016/j.marpolbul.2019.04.034

Babcsányi, I., Chabaux, F., Granet, M., Meite, F., Payraudeau, S., Duplay, J., Imfeld, G., 2016. Copper in soil fractions and runoff in a vineyard catchment: Insights from copper stable isotopes. *Science of The Total Environment* 557–558, 154–162. https://doi.org/10.1016/j.scitotenv.2016.03.037

Babcsányi, I., Imfeld, G., Granet, M., Chabaux, F., 2014. Copper Stable Isotopes To Trace Copper Behavior in Wetland Systems. *Environ. Sci. Technol*. 48, 5520–5529. https://doi.org/10.1021/es405688v

Balistrieri, L.S., Borrok, D.M., Wanty, R.B., Ridley, W.I., 2008. Fractionation of Cu and Zn isotopes during adsorption onto amorphous Fe(III) oxyhydroxide: Experimental mixing of acid rock drainage and ambient river water. *Geochimica et Cosmochimica Acta* 72, 311–328. https://doi.org/10.1016/j.gca.2007.11.013

Barletta, M., Lima, A.R.A., Costa, M.F., 2019. Distribution, sources and consequences of nutrients, persistent organic pollutants, metals and microplastics in South American estuaries. *Science of The Total Environment* 651, 1199–1218. https://doi.org/10.1016/j.scitotenv.2018.09.276

Bausinger, T., Bonnaire, E., Preuß, J., 2007. Exposure assessment of a burning ground for chemical ammunition on the Great War battlefields of Verdun. *Science of The Total Environment* 382, 259–271. https://doi.org/10.1016/j.scitotenv.2007.04.029

Bigalke, M., Weyer, S., Wilcke, W., 2010. Copper Isotope Fractionation during Complexation with Insolubilized Humic Acid. *Environ. Sci. Technol.* 44, 5496–5502. https://doi.org/10.1021/es1017653

Briant, N., Chouvelon, T., Martinez, L., Brach-Papa, C., Chiffoleau, J., Savoye, N., Sonke, J., Knoery, J., 2017. Spatial and temporal distribution of mercury and methylmercury in bivalves from the French coastline. *Marine Pollution Bulletin* 114, 1096–1102. https://doi.org/10.1016/j.marpolbul.2016.10.018

Burdige, D.J., 2007. Biogeochemistry of Estuaries. Eos Trans. AGU 88, 581. https://doi.org/10.1029/2007EO520011

Charalampides, G., Manoliadis, O., 2002. Sr and Pb isotopes as environmental indicators in environmental studies. *Environment International* 28, 147–151. https://doi.org/10.1016/S0160-4120(02)00020-X

Chen, C.-W., Kao, C.-M., Chen, C.-F., Dong, C.-D., 2007a. Distribution and accumulation of heavy metals in the sediments of Kaohsiung Harbor, Taiwan. *Chemosphere* 66, 1431–1440. https://doi.org/10.1016/j.chemosphere.2006.09.030

Chen, C.-W., Kao, C.-M., Chen, C.-F., Dong, C.-D., 2007b. Distribution and accumulation of heavy metals in the sediments of Kaohsiung Harbor, Taiwan. *Chemosphere* 66, 1431–1440. https://doi.org/10.1016/j.chemosphere.2006.09.030

Chen, H., Savage, P.S., Teng, F.-Z., Helz, R.T., Moynier, F., 2013. Zinc isotope fractionation during magmatic differentiation and the isotopic composition of the bulk Earth. *Earth and Planetary Science Letters* 369–370, 34–42. https://doi.org/10.1016/j.epsl.2013.02.037

Chouvelon, T., Cresson, P., Bouchoucha, M., Brach-Papa, C., Bustamante, P., Crochet, S., Marco-Miralles, F., Thomas, B., Knoery, J., 2018. Oligotrophy as a major driver of mercury bioaccumulation in medium- to high-trophic level consumers: A marine ecosystem-comparative study. *Environmental Pollution* 233, 844–854. https://doi.org/10.1016/j.envpol.2017.11.015

Cloquet, C., Carignan, J., Libourel, G., 2006. Isotopic Composition of Zn and Pb Atmospheric Depositions in an Urban/Periurban Area of Northeastern France. *Environ. Sci. Technol.* 40, 6594–6600. https://doi.org/10.1021/es0609654

Coclet, C., Garnier, C., Delpy, F., Jamet, D., Durrieu, G., Le Poupon, C., Mayer, M., Misson, B., 2018. Trace metal contamination as a toxic and structuring factor impacting ultraphytoplankton communities in a multicontaminated Mediterranean coastal area. *Progress in Oceanography* 163, 196–213. https://doi.org/10.1016/j.pocean.2017.06.006

Cossa, D., Garnier, C., Buscail, R., Elbaz-Poulichet, F., Mikac, N., Patel-Sorrentino, N., Tessier, E., Rigaud, S., Lenoble, V., Gobeil, C., 2014. A Michaelis–Menten type equation for describing methylmercury dependence on inorganic mercury in aquatic sediments. *Biogeochemistry* 119, 35–43. https://doi.org/10.1007/s10533-013-9924-3

Dang, D.H., Lenoble, V., Durrieu, G., Omanović, D., Mullot, J.-U., Mounier, S., Garnier, C., 2015a. Seasonal variations of coastal sedimentary trace metals cycling: Insight on the effect of manganese and iron (oxy)hydroxides, sulphide and organic matter. *Marine Pollution Bulletin* 92, 113–124.

https://doi.org/10.1016/j.marpolbul.2014.12.048
Dang, D.H., Schäfer, J., Brach-Papa, C., Lenoble, V., Durrieu, G., Dutruch, L., Chiffoleau, J.-F., Gonzalez, J.-L., Blanc, G., Mullot, J.-U., Mounier, S., Garnier, C., 2015b. Evidencing the Impact of Coastal Contaminated Sediments on Mussels Through Pb Stable Isotopes Composition. *Environ. Sci. Technol*. 49, 11438–11448. https://doi.org/10.1021/acs.est.5b01893
de Souza Machado, A.A., Spencer, K., Kloas, W., Toffolon, M., Zarfl, C., 2016. Metal fate and effects in estuaries: A review and conceptual model for better understanding of toxicity. *Science of The Total Environment* 541, 268–281. https://doi.org/10.1016/j.scitotenv.2015.09.045
Dekov, V.M., Vanlierde, E., Billström, K., Garbe-Schönberg, C.-D., Weiss, D.J., Gatto Rotondo, G., Van Meel, K., Kuzmann, E., Fortin, D., Darchuk, L., Van Grieken, R., 2014. Ferrihydrite precipitation in groundwater-fed river systems (Nete and Demer river basins, Belgium): Insights from a combined Fe-Zn-Sr-Nd-Pb-isotope study. *Chemical Geology* 386, 1–15. https://doi.org/10.1016/j.chemgeo.2014.07.023
Deng, T.-H.-B., Cloquet, C., Tang, Y.-T., Sterckeman, T., Echevarria, G., Estrade, N., Morel, J.-L., Qiu, R.-L., 2014. Nickel and Zinc Isotope Fractionation in Hyperaccumulating and Nonaccumulating Plants. *Environ. Sci. Technol.* 48, 11926–11933. https://doi.org/10.1021/es5020955
Dolgopolova, A., Weiss, D.J., Seltmann, R., Kober, B., Mason, T.F.D., Coles, B., Stanley, C.J., 2006. Use of isotope ratios to assess sources of Pb and Zn dispersed in the environment during mining and ore processing within the Orlovka–Spokoinoe mining site (Russia). *Applied Geochemistry* 21, 563–579. https://doi.org/10.1016/j.apgeochem.2005.12.014
Doucet, L.S., Laurent, O., Mattielli, N., Debouge, W., 2018. Zn isotope heterogeneity in the continental lithosphere: New evidence from Archean granitoids of the northern Kaapvaal craton, South Africa. *Chemical Geology* 476, 260–271. https://doi.org/10.1016/j.chemgeo.2017.11.022
Ducher, M., Blanchard, M., Balan, E., 2016. Equilibrium zinc isotope fractionation in Zn-bearing minerals from first-principles calculations. *Chemical Geology* 443, 87–96. https://doi.org/10.1016/j.chemgeo.2016.09.016
El Azzi, D., Viers, J., Guiresse, M., Probst, A., Aubert, D., Caparros, J., Charles, F., Guizien, K., Probst, J.L., 2013. Origin and fate of copper in a small Mediterranean vineyard catchment: New insights from combined chemical extraction and δ65Cu isotopic composition. *Science of The Total Environment* 463–464, 91–101. https://doi.org/10.1016/j.scitotenv.2013.05.058
Field, A., 2017. Discovering Statistics Using IBM SPSS Statistics: North American Edition.
Gonzalez, R., Weiss, D., 2015. Zinc Isotope Variability in Three Coal-Fired Power Plants: A Predictive Model for Determining Isotopic Fractionation during Combustion. *Environ. Sci. Technol.* 49, 12560–12567. https://doi.org/10.1021/acs.est.5b02402
Gonzalez, R.O., Strekopytov, S., Amato, F., Querol, X., Reche, C., Weiss, D., 2016. New Insights from Zinc and Copper Isotopic Compositions into the Sources of Atmospheric Particulate Matter from Two Major European Cities. *Environ. Sci. Technol.* 50, 9816–9824. https://doi.org/10.1021/acs.est.6b00863
Guinoiseau, D., Bouchez, J., Gélabert, A., Louvat, P., Moreira-Turcq, P., Filizola, N., Benedetti, M.F., 2018a. Fate of particulate copper and zinc isotopes at the Solimões-Negro river confluence, Amazon Basin, Brazil. *Chemical Geology* 489, 1–15. https://doi.org/10.1016/j.chemgeo.2018.05.004
Guinoiseau, D., Bouchez, J., Gélabert, A., Louvat, P., Moreira-Turcq, P., Filizola, N., Benedetti, M.F., 2018b. Fate of particulate copper and zinc isotopes at the Solimões-Negro river confluence, Amazon Basin, Brazil. *Chemical Geology* 489, 1–15. https://doi.org/10.1016/j.chemgeo.2018.05.004
Guinoiseau, D., Gélabert, A., Allard, T., Louvat, P., Moreira-Turcq, P., Benedetti, M.F., 2017. Zinc and copper behaviour at the soil-river interface: New insights by Zn and Cu isotopes in the organic-rich Rio Negro basin. *Geochimica et Cosmochimica Acta* 213, 178–197. https://doi.org/10.1016/j.gca.2017.06.030

Guinoiseau, D., Gélabert, A., Moureau, J., Louvat, P., Benedetti, M.F., 2016. Zn Isotope Fractionation during Sorption onto Kaolinite. *Environ. Sci. Technol.* 50, 1844–1852. https://doi.org/10.1021/acs.est.5b05347

Inglis, E.C., Debret, B., Burton, K.W., Millet, M.-A., Pons, M.-L., Dale, C.W., Bouilhol, P., Cooper, M., Nowell, G.M., McCoy-West, A.J., Williams, H.M., 2017. The behavior of iron and zinc stable isotopes accompanying the subduction of mafic oceanic crust: A case study from Western Alpine ophiolites: Fe and Zn isotopes during subduction. *Geochem. Geophys. Geosyst.* 18, 2562–2579. https://doi.org/10.1002/2016GC006735

Jamieson-Hanes, J.H., Shrimpton, H.K., Veeramani, H., Ptacek, C.J., Lanzirotti, A., Newville, M., Blowes, D.W., 2017. Evaluating zinc isotope fractionation under sulfate reducing conditions using a flow-through cell and in situ XAS analysis. *Geochimica et Cosmochimica Acta* 203, 1–14. https://doi.org/10.1016/j.gca.2016.12.034

Jansen, M., Hauptmann, A., Klein, S., Seitz, H.-M., 2018. The potential of stable Cu isotopes for the identification of Bronze Age ore mineral sources from Cyprus and Faynan: results from Uluburun and Khirbat Hamra Ifdan. *Archaeol Anthropol Sci* 10, 1485–1502. https://doi.org/10.1007/s12520-017-0465-x

Jean, N., Dumont, E., Durrieu, G., Balliau, T., Jamet, J.-L., Personnic, S., Garnier, C., 2012. Protein expression from zooplankton communities in a metal contaminated NW mediterranean coastal ecosystem. *Marine Environmental Research* 80, 12–26. https://doi.org/10.1016/j.marenvres.2012.06.004

John, S.G., Genevieve Park, J., Zhang, Z., Boyle, E.A., 2007. The isotopic composition of some common forms of anthropogenic zinc. *Chemical Geology* 245, 61–69. https://doi.org/10.1016/j.chemgeo.2007.07.024

John, S.G., Kunzmann, M., Townsend, E.J., Rosenberg, A.D., 2017. Zinc and cadmium stable isotopes in the geological record: A case study from the post-snowball Earth Nuccaleena cap dolostone. *Palaeogeography, Palaeoclimatology, Palaeoecology* 466, 202–208. https://doi.org/10.1016/j.palaeo.2016.11.003

Kavner, A., John, S.G., Sass, S., Boyle, E.A., 2008. Redox-driven stable isotope fractionation in transition metals: Application to Zn electroplating. *Geochimica et Cosmochimica Acta* 72, 1731–1741. https://doi.org/10.1016/j.gca.2008.01.023

Komárek, M., Ettler, V., Chrastný, V., Mihaljevič, M., 2008. Lead isotopes in environmental sciences: A review. *Environment International* 34, 562–577. https://doi.org/10.1016/j.envint.2007.10.005

Kunzmann, M., Halverson, G.P., Sossi, P.A., Raub, T.D., Payne, J.L., Kirby, J., 2013. Zn isotope evidence for immediate resumption of primary productivity after snowball Earth. *Geology* 41, 27–30. https://doi.org/10.1130/G33422.1

Little, S.H., Vance, D., McManus, J., Severmann, S., 2016. Key role of continental margin sediments in the oceanic mass balance of Zn and Zn isotopes. *Geology* 44, 207–210. https://doi.org/10.1130/G37493.1

Little, S.H., Vance, D., Walker-Brown, C., Landing, W.M., 2014. The oceanic mass balance of copper and zinc isotopes, investigated by analysis of their inputs, and outputs to ferromanganese oxide sediments. *Geochimica et Cosmochimica Acta* 125, 673–693. https://doi.org/10.1016/j.gca.2013.07.046

Liu, S.-A., Huang, J., Liu, J., Wörner, G., Yang, W., Tang, Y.-J., Chen, Y., Tang, L., Zheng, J., Li, S., 2015. Copper isotopic composition of the silicate Earth. *Earth and Planetary Science Letters* 427, 95–103. https://doi.org/10.1016/j.epsl.2015.06.061

Lv, Y., Liu, S.-A., Zhu, J.-M., Li, S., 2016. Copper and zinc isotope fractionation during deposition and weathering of highly metalliferous black shales in central China. *Chemical Geology* 445, 24–35. https://doi.org/10.1016/j.chemgeo.2016.01.016

Machado, W., Santelli, R.E., Carvalho, M.F., Molisani, M.M., Barreto, R.C., Lacerda, L.D., 2008. Relation of Reactive Sulfides with Organic Carbon, Iron, and Manganese in Anaerobic Mangrove Sediments: Implications for Sediment Suitability to Trap Trace Metals. *Journal of Coastal Research* 4, 25–32. https://doi.org/10.2112/06-0736.1

Mar da Costa, N.Y., Boaventura, G.R., Mulholland, D.S., Araújo, D.F., Moreira, R.C.A., Faial, K.C.F., Bomfim, E. de O., 2016. Biogeochemical mechanisms controlling trophic state and micropollutant

concentrations in a tropical artificial lake. *Environ Earth Sci* 75, 854. https://doi.org/10.1007/s12665-016-5629-y

Maréchal, C.N., Télouk, P., Albarède, F., 1999. Precise analysis of copper and zinc isotopic compositions by plasma-source mass spectrometry. *Chemical Geology* 156, 251–273. https://doi.org/10.1016/S0009-2541(98)00191-0

Mason, R.P., 2013. Trace Metals in Aquatic Systems: Mason/Trace Metals in Aquatic Systems. John Wiley & Sons, Ltd, Chichester, UK. https://doi.org/10.1002/9781118274576

Mattielli, N., Petit, J.C.J., Deboudt, K., Flament, P., Perdrix, E., Taillez, A., Rimetz-Planchon, J., Weis, D., 2009. Zn isotope study of atmospheric emissions and dry depositions within a 5 km radius of a Pb–Zn refinery. *Atmospheric Environment* 43, 1265–1272. https://doi.org/10.1016/j.atmosenv.2008.11.030

Meglen, R.R., 1992. Examining large databases: a chemometric approach using principal component analysis. *Marine Chemistry* 39, 217–237. https://doi.org/10.1016/0304-4203(92)90103-H

Misson, B., Garnier, C., Lauga, B., Dang, D.H., Ghiglione, J.-F., Mullot, J.-U., Duran, R., Pringault, O., 2016. Chemical multi-contamination drives benthic prokaryotic diversity in the anthropized Toulon Bay. *Science of The Total Environment* 556, 319–329. https://doi.org/10.1016/j.scitotenv.2016.02.038

Mondillo, N., Wilkinson, J.J., Boni, M., Weiss, D.J., Mathur, R., 2018. A global assessment of Zn isotope fractionation in secondary Zn minerals from sulfide and non-sulfide ore deposits and model for fractionation control. *Chemical Geology* 500, 182–193. https://doi.org/10.1016/j.chemgeo.2018.09.033

Mortimer, R.J.G., Rae, J.E., 2000. Metal Speciation (Cu, Zn, Pb, Cd) and Organic Matter in Oxic to Suboxic Salt Marsh Sediments, Severn Estuary, Southwest Britain. *Marine Pollution Bulletin* 40, 377–386. https://doi.org/10.1016/S0025-326X(99)00176-9

Moynier, F., Vance, D., Fujii, T., Savage, P., 2017. The Isotope Geochemistry of Zinc and Copper. *Reviews in Mineralogy and Geochemistry* 82, 543–600. https://doi.org/10.2138/rmg.2017.82.13

Mulholland, D.S., Boaventura, G.R., Araújo, D.F., 2012. Geological and anthropogenic influences on sediment metal composition in the upper Paracatu River Basin, Brazil. *Environ Earth Sci* 67, 1307–1317. https://doi.org/10.1007/s12665-012-1574-6

Naser, H.A., 2013. Assessment and management of heavy metal pollution in the marine environment of the Arabian Gulf: A review. *Marine Pollution Bulletin* 72, 6–13. https://doi.org/10.1016/j.marpolbul.2013.04.030

Petit, J.C.J., Schäfer, J., Coynel, A., Blanc, G., Deycard, V.N., Derriennic, H., Lanceleur, L., Dutruch, L., Bossy, C., Mattielli, N., 2013. Anthropogenic sources and biogeochemical reactivity of particulate and dissolved Cu isotopes in the turbidity gradient of the Garonne River (France). *Chemical Geology* 359, 125–135. https://doi.org/10.1016/j.chemgeo.2013.09.019

Pokrovsky, O.S., Viers, J., Emnova, E.E., Kompantseva, E.I., Freydier, R., 2008. Copper isotope fractionation during its interaction with soil and aquatic microorganisms and metal oxy(hydr)oxides: Possible structural control. *Geochimica et Cosmochimica Acta* 72, 1742–1757. https://doi.org/10.1016/j.gca.2008.01.018

Pougnet, F., Schäfer, J., Dutruch, L., Garnier, C., Tessier, E., Dang, D.H., Lanceleur, L., Mullot, J.-U., Lenoble, V., Blanc, G., 2014. Sources and historical record of tin and butyl-tin species in a Mediterranean bay (Toulon Bay, France). *Environ Sci Pollut Res* 21, 6640–6651. https://doi.org/10.1007/s11356-014-2576-6

Ratié, G., Jouvin, D., Garnier, J., Rouxel, O., Miska, S., Guimarães, E., Cruz Vieira, L., Sivry, Y., Zelano, I., Montarges-Pelletier, E., Thil, F., Quantin, C., 2015. Nickel isotope fractionation during tropical weathering of ultramafic rocks. *Chemical Geology* 402, 68–76. https://doi.org/10.1016/j.chemgeo.2015.02.039

Rossi, N., Jamet, J.-L., 2008. In situ heavy metals (copper, lead and cadmium) in different plankton compartments and suspended particulate matter in two coupled Mediterranean coastal ecosystems

(Toulon Bay, France). *Marine Pollution Bulletin* 56, 1862–1870. https://doi.org/10.1016/j.marpolbul.2008.07.018

Savage, P.S., Moynier, F., Chen, H., Shofner, G., Siebert, J., Badro, J., Puchtel, I.S., 2015. Copper isotope evidence for large-scale sulphide fractionation during Earth's differentiation. *Geochem. Persp. Let.* 53–64. https://doi.org/10.7185/geochemlet.1506

Shiel, A.E., Weis, D., Orians, K.J., 2010. Evaluation of zinc, cadmium and lead isotope fractionation during smelting and refining. *Science of The Total Environment* 408, 2357–2368. https://doi.org/10.1016/j.scitotenv.2010.02.016

Šillerová, H., Chrastný, V., Vítková, M., Francová, A., Jehlička, J., Gutsch, M.R., Kocourková, J., Aspholm, P.E., Nilsson, L.O., Berglen, T.F., Jensen, H.K.B., Komárek, M., 2017. Stable isotope tracing of Ni and Cu pollution in North-East Norway: Potentials and drawbacks. *Environmental Pollution* 228, 149–157. https://doi.org/10.1016/j.envpol.2017.05.030

Sivry, Y., Riotte, J., Sonke, J.E., Audry, S., Schäfer, J., Viers, J., Blanc, G., Freydier, R., Dupré, B., 2008. Zn isotopes as tracers of anthropogenic pollution from Zn-ore smelters The Riou Mort–Lot River system. *Chemical Geology* 255, 295–304. https://doi.org/10.1016/j.chemgeo.2008.06.038

Souto-Oliveira, C.E., Babinski, M., Araújo, D.F., Andrade, M.F., 2018. Multi-isotopic fingerprints (Pb, Zn, Cu) applied for urban aerosol source apportionment and discrimination. *Science of The Total Environment* 626, 1350–1366. https://doi.org/10.1016/j.scitotenv.2018.01.192

Souto-Oliveira, C.E., Babinski, M., Araújo, D.F., Weiss, D.J., Ruiz, I.R., 2019. Multi-isotope approach of Pb, Cu and Zn in urban aerosols and anthropogenic sources improves tracing of the atmospheric pollutant sources in megacities. *Atmospheric Environment* 198, 427–437. https://doi.org/10.1016/j.atmosenv.2018.11.007

Sparks, D.L., 2005. Toxic Metals in the Environment: The Role of Surfaces. Elements 1, 193–197. https://doi.org/10.2113/gselements.1.4.193

Suhr, N., Schoenberg, R., Chew, D., Rosca, C., Widdowson, M., Kamber, B.S., 2018. Elemental and isotopic behaviour of Zn in Deccan basalt weathering profiles: Chemical weathering from bedrock to laterite and links to Zn deficiency in tropical soils. *Science of The Total Environment* 619–620, 1451–1463. https://doi.org/10.1016/j.scitotenv.2017.11.112

Tessier, E., Garnier, C., Mullot, J.-U., Lenoble, V., Arnaud, M., Raynaud, M., Mounier, S., 2011. Study of the spatial and historical distribution of sediment inorganic contamination in the Toulon bay (France). *Marine Pollution Bulletin* 62, 2075–2086. https://doi.org/10.1016/j.marpolbul.2011.07.022

Thapalia, A., Borrok, D.M., Van Metre, P.C., Wilson, J., 2015. Zinc Isotopic Signatures in Eight Lake Sediment Cores from Across the United States. *Environ. Sci. Technol.* 49, 132–140. https://doi.org/10.1021/es5036893

Turner, A., Millward, G.E., 2002. Suspended Particles: Their Role in Estuarine Biogeochemical Cycles. Estuarine, *Coastal and Shelf Science* 55, 857–883. https://doi.org/10.1006/ecss.2002.1033

Veeramani, H., Eagling, J., Jamieson-Hanes, J.H., Kong, L., Ptacek, C.J., Blowes, D.W., 2015. Zinc Isotope Fractionation as an Indicator of Geochemical Attenuation Processes. *Environ. Sci. Technol. Lett.* 2, 314–319. https://doi.org/10.1021/acs.estlett.5b00273

Viers, J., Grande, J.A., Zouiten, C., Freydier, R., Masbou, J., Valente, T., Torre, M.-L. de la, Destrigneville, C., Pokrovsky, O.S., 2018. Are Cu isotopes a useful tool to trace metal sources and processes in acid mine drainage (AMD) context? *Chemosphere* 193, 1071–1079. https://doi.org/10.1016/j.chemosphere.2017.11.133

Wang, Z.-Z., Liu, S.-A., Liu, J., Huang, J., Xiao, Y., Chu, Z.-Y., Zhao, X.-M., Tang, L., 2017. Zinc isotope fractionation during mantle melting and constraints on the Zn isotope composition of Earth's upper mantle. *Geochimica et Cosmochimica* Acta 198, 151–167. https://doi.org/10.1016/j.gca.2016.11.014

Yin, N.-H., Sivry, Y., Benedetti, M.F., Lens, P.N.L., van Hullebusch, E.D., 2016. Application of Zn isotopes in environmental impact assessment of Zn–Pb metallurgical industries: A mini review. *Applied Geochemistry* 64, 128–135. https://doi.org/10.1016/j.apgeochem.2015.09.016

Zhang, R., Russell, J., Xiao, X., Zhang, F., Li, T., Liu, Z., Guan, M., Han, Q., Shen, L., Shu, Y., 2018. Historical records, distributions and sources of mercury and zinc in sediments of East China sea: Implication from stable isotopic compositions. *Chemosphere* 205, 698–708. https://doi.org/10.1016/j.chemosphere.2018.04.100

Zhou, Q., Zhang, J., Fu, J., Shi, J., Jiang, G., 2008. Biomonitoring: An appealing tool for assessment of metal pollution in the aquatic ecosystem. *Analytica Chimica Acta* 606, 135–150. https://doi.org/10.1016/j.aca.2007.11.018

Zuykov, M., Pelletier, E., Harper, D.A.T., 2013. Bivalve mollusks in metal pollution studies: From bioaccumulation to biomonitoring. *Chemosphere* 93, 201–208. https://doi.org/10.1016/j.chemosphere.2013.05.001

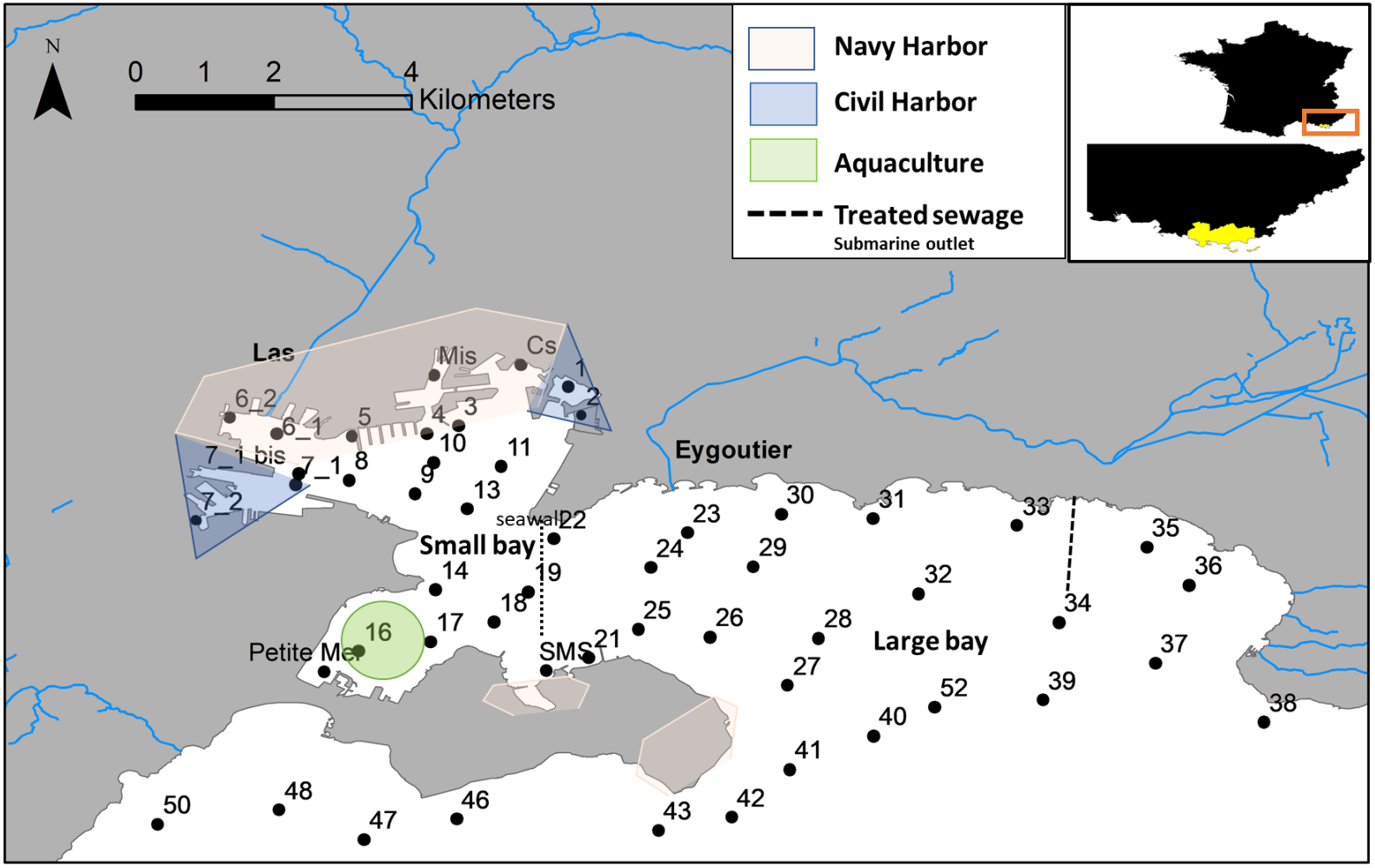

Fig. 1. Map of Toulon bay and sampling sites of surface sediments.

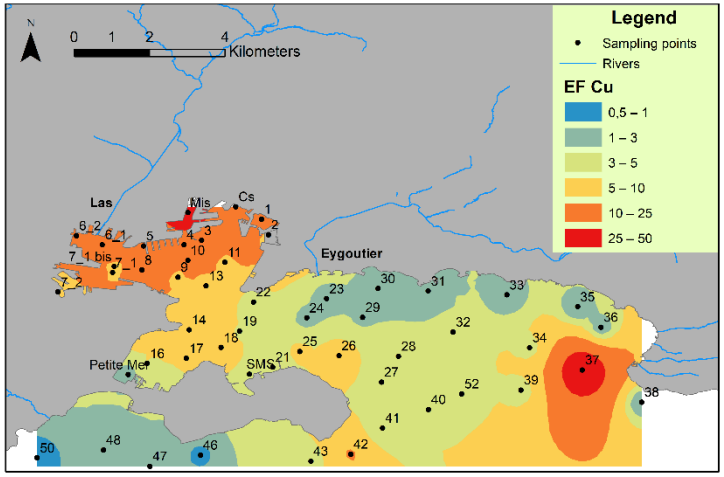
N
0 1 2 4
Kilometers
Legend
Sampling points
Rivers
EF Cu
0,5 – 1
1 – 3
3 – 5
5 – 10
10 – 25
25 – 50
Las
Mis
Cs
Eygoutier
Petite Mer
SMS

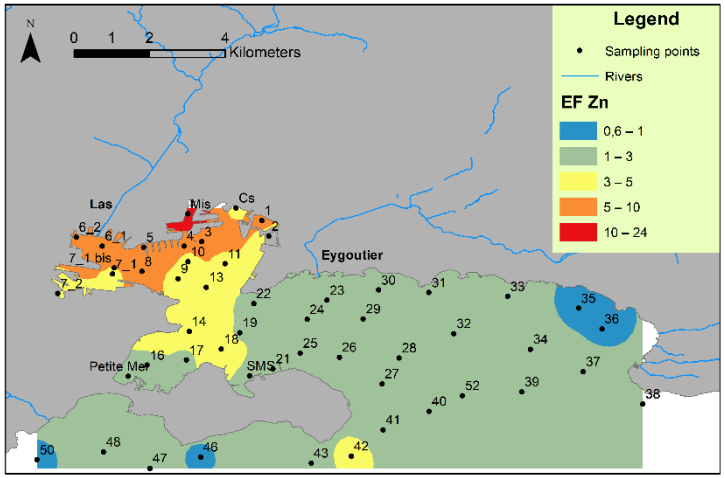
N
0 1 2 4
Kilometers
Legend
Sampling points
Rivers
EF Zn
0,6 – 1
1 – 3
3 – 5
5 – 10
10 – 24
Las
Mis
Cs
Eygoutier
Petite Mer
SMS

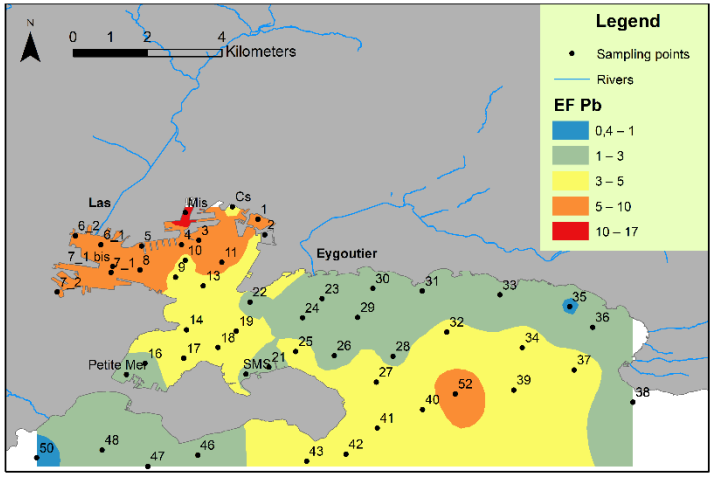
N
0 1 2 4
Kilometers
Legend
Sampling points
Rivers
EF Pb
0,4 – 1
1 – 3
3 – 5
5 – 10
10 – 17
Las
Mis
Cs
Eygoutier
Petite Mer
SMS

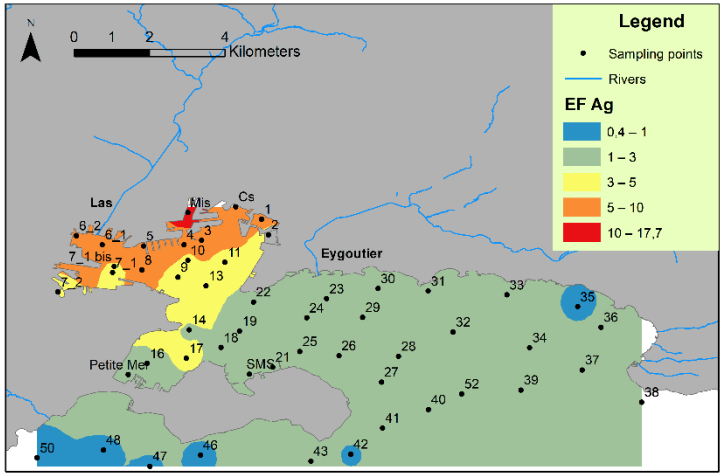
N
0 1 2 4
Kilometers
Legend
Sampling points
Rivers
EF Ag
0,4 – 1
1 – 3
3 – 5
5 – 10
10 – 17,7
Las
Mis
Cs
Eygoutier
Petite Mer
SMS

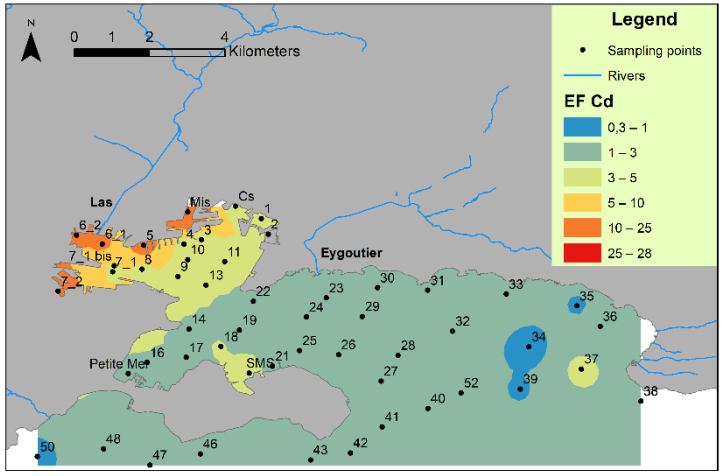
N
0 1 2 4
Kilometers
Legend
Sampling points
Rivers
EF Cd
0,3 – 1
1 – 3
3 – 5
5 – 10
10 – 25
25 – 28
Las
Mis
Cs
Eygoutier
Petite Mer
SMS

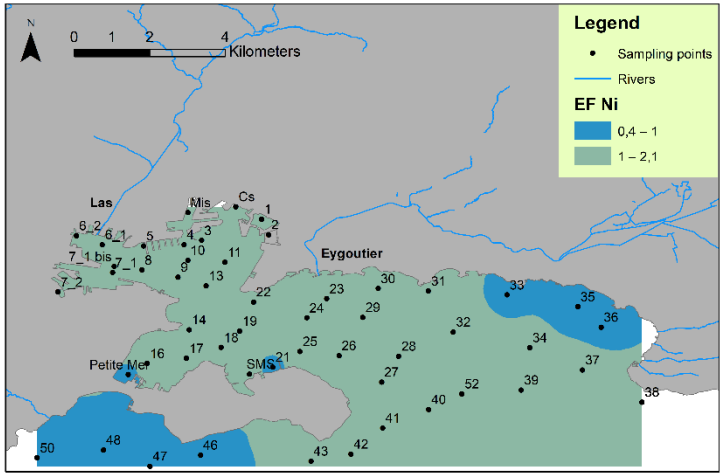
N
0 1 2 4
Kilometers
Legend
Sampling points
Rivers
EF Ni
0,4 – 1
1 – 2,1
Las
Mis
Cs
Eygoutier
Petite Mer
SMS

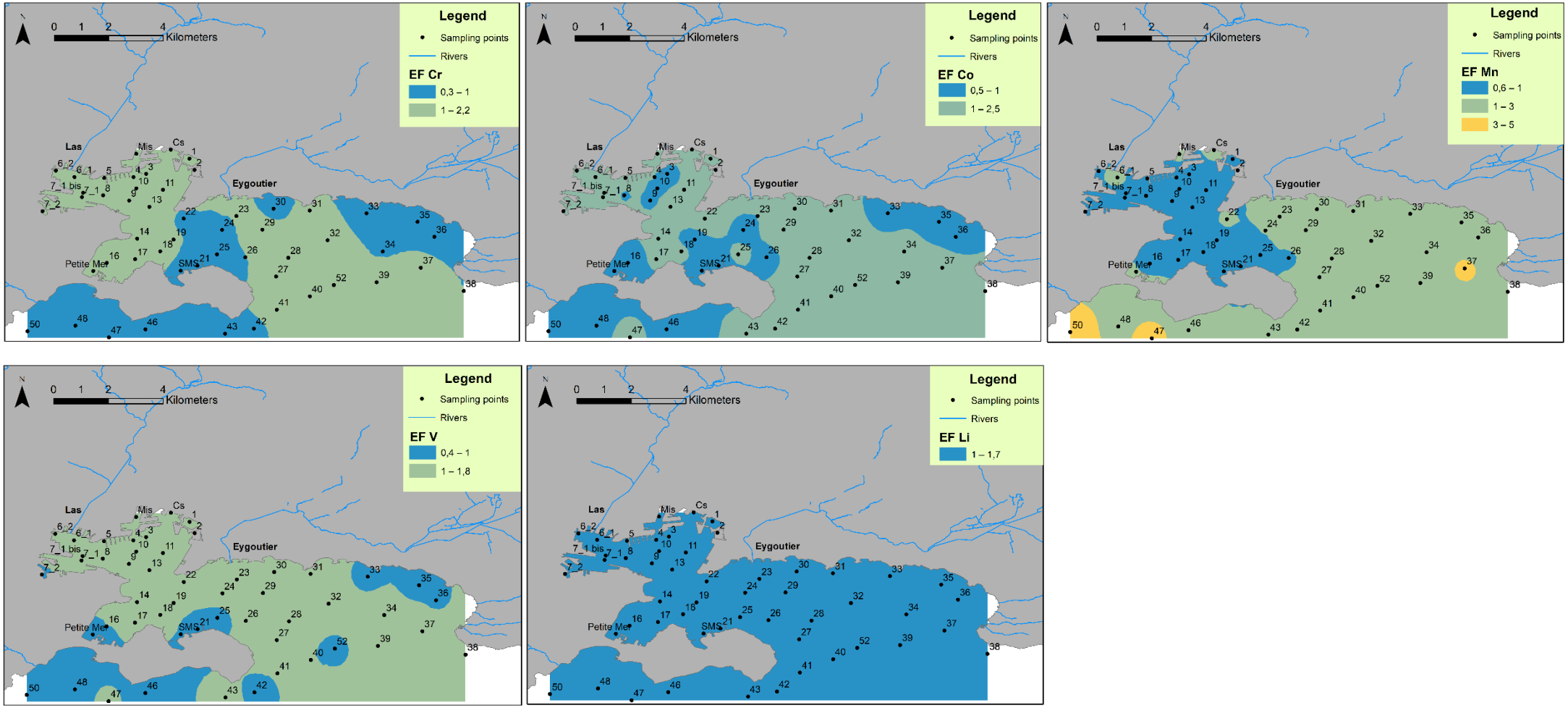

Fig. 2. Interpolation maps of trace elements enrichment factors (EF) in surface sediments. Enrichment factor values were classed as suggested in other studies (Chen *et al.*, 2007): EF < 1 indicates no enrichment; EF < 3 for minor enrichment; EF = 3–5 for moderate enrichment; EF = 5–10 for moderately severe enrichment; EF = 10–25 for severe enrichment; EF = 25–50 for very severe enrichment; and EF > 50 for extremely severe enrichment.

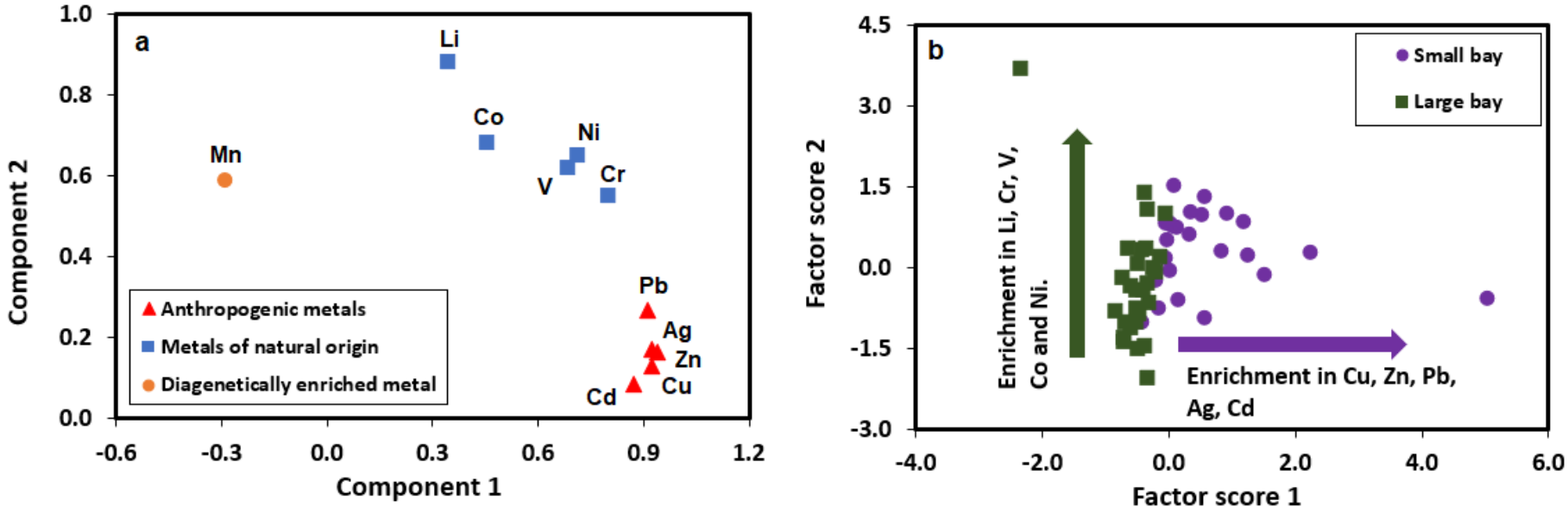

Fig. 3. Principal component analysis of surface sediments from Toulon bay: (a) the main components and factor loads; (b) the sample factor scores.

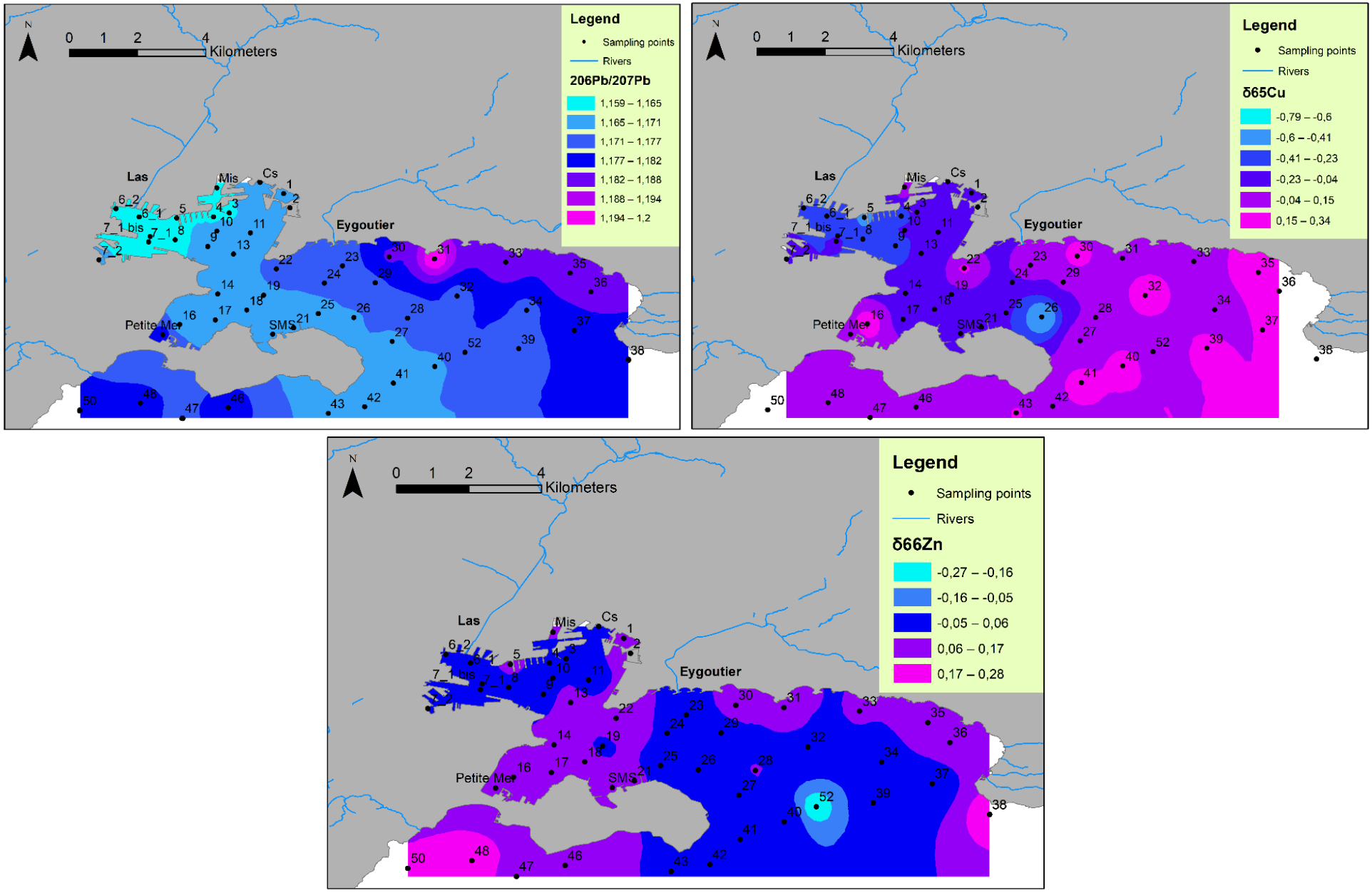

Fig. 4. Interpolation map of isotope compositions of Pb, Cu and Zn in surface sediments.

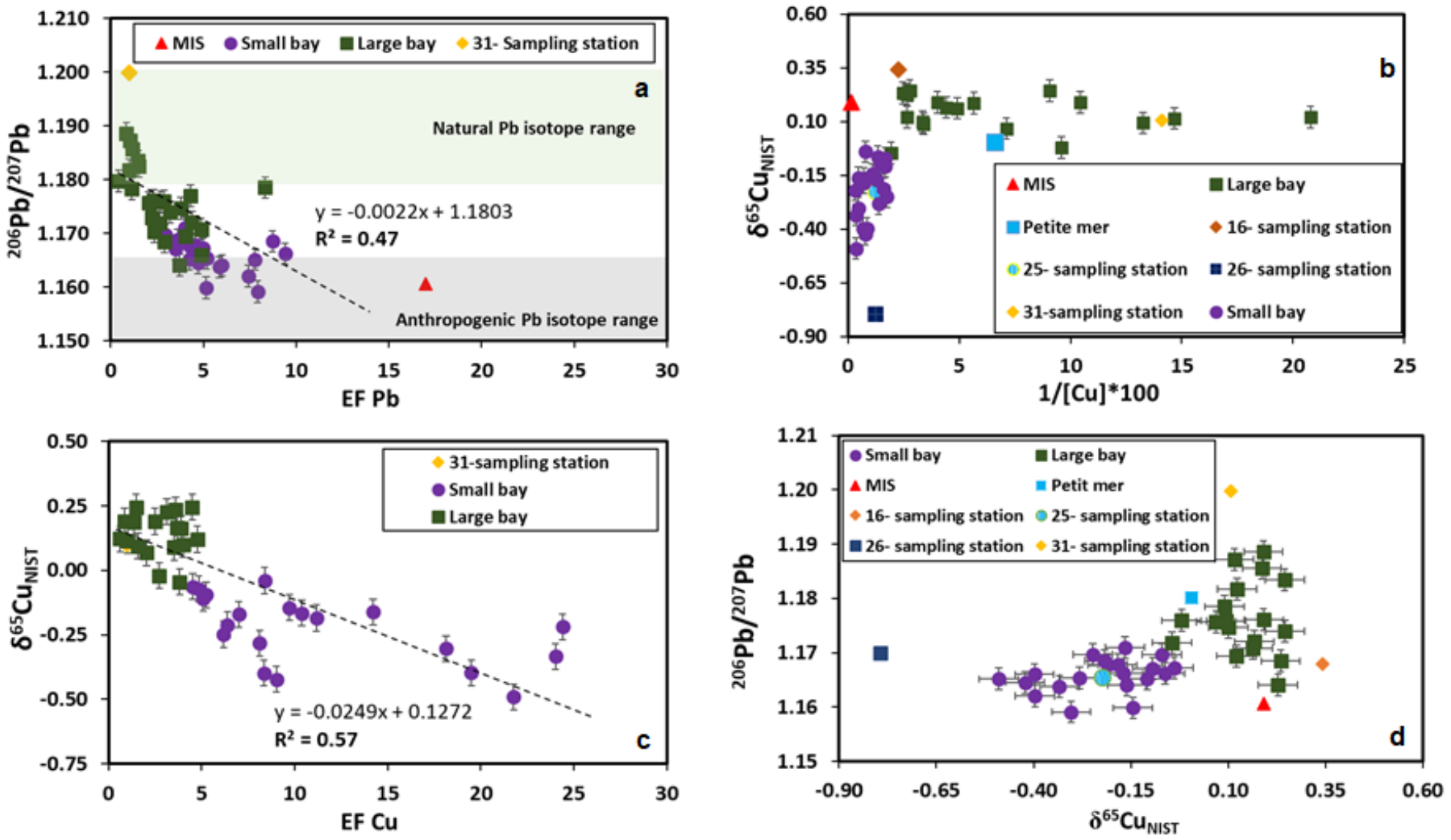

Fig. 5. Plots of elemental and isotope data of Cu and Pb. Copper concentrations [Cu] are expressed in µg. g^{-1}.

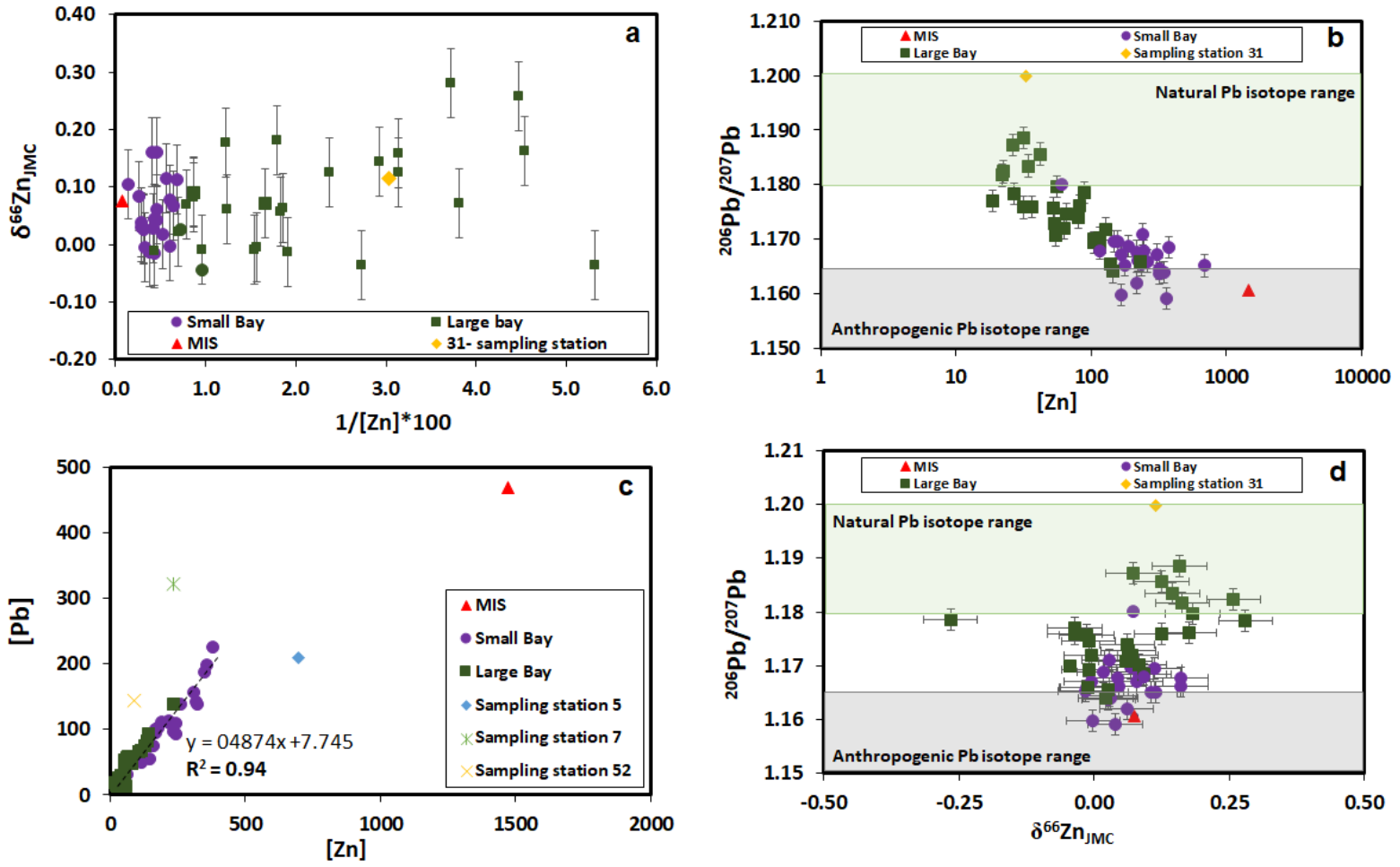

Fig. 6. Plots of elemental and isotope data of Zn. Zinc concentrations [Zn] are expressed in µg. g^{-1}.

Table 1. Copper, zinc and lead data description of Toulon bay sediments.

All Toulon bay						
	n	**Range**	**Minimum**	**Maximum**	**Mean**	**Std. Deviation (1s)**
δ^{65}Cu (‰)	44	1.13	-0.79	0.34	-0.05	0.24
δ^{66}Zn (‰)	52	0.55	-0.27	0.28	0.06	0.09
^{206}Pb/^{207}Pb	52	0.0407	1.1591	1.1998	1.1717	0.0081
Cu (µg.g^{-1})	52	662	4	666	85	111
Zn (µg.g^{-1})	52	1452	19	1471	178	223
Pb (µg.g^{-1})	52	456	13	470	93	83
Small bay						
	n	**Range**	**Minimum**	**Maximum**	**Mean**	**Std. Deviation (1s)**
δ^{65}Cu (‰)	23	0.83	-0.49	0.34	-0.17	0.19
δ^{66}Zn (‰)	24	0.18	-0.02	0.16	0.06	0.05
^{206}Pb/^{207}Pb	24	0.0210	1.1591	1.1801	1.1664	0.0043
Cu (µg.g^{-1})	24	651	15	666	147	137
Zn (µg.g^{-1})	24	1411	60	1471	302	278
Pb (µg.g^{-1})	24	438	32	470	144	94
Large bay						
	n	**Range**	**Minimum**	**Maximum**	**Mean**	**Std. Deviation (1s)**
δ^{65}Cu (‰)	21	1.03	-0.79	0.24	0.08	0.23
δ^{66}Zn (‰)	28	0.55	-0.27	0.28	0.06	0.11
^{206}Pb/^{207}Pb	28	0.0357	1.1641	1.1998	1.1763	0.0079
Cu (µg.g^{-1})	28	141	4	145	32	32
Zn (µg.g^{-1})	28	214	19	233	72	50
Pb (µg.g^{-1})	28	131	13	145	49	35